Chemistry & Biology, Vol. 9, 171–184, February, 2002, ©2002 Elsevier Science Ltd. All rights reserved. PII S1074-5521(02)00100-X

Conversion of L-Proline to Pyrrolyl-2-Carboxyl-*S*-PCP during Undecylprodigiosin and Pyoluteorin Biosynthesis

Michael G. Thomas, Michael D. Burkart, and Christopher T. Walsh[1]
Department of Biological Chemistry and Molecular Pharmacology
Harvard Medical School
240 Longwood Avenue
Boston, MA 02115

Summary

Several medically and agriculturally important natural products contain pyrrole moieties. Precursor labeling studies of some of these natural products have shown that L-proline can serve as the biosynthetic precursor for these moieties, including those found in coumermycin A_1, pyoluteorin, and one of the pyrroles of undecylprodigiosin. This suggests a novel mechanism for pyrrole biosynthesis. The biosynthetic gene clusters for these three natural products each encode proteins homologous to adenylation (A) and peptidyl carrier protein (PCP) domains of nonribosomal peptide synthetases in addition to novel acyl-CoA dehydrogenases. Here we show that the three proteins from the undecylprodigiosin and pyoluteorin biosynthetic pathways are sufficient for the conversion of L-proline to pyrrolyl-2-carboxyl-*S*-PCP. This establishes a novel mechanism for pyrrole biosynthesis and extends the hypothesis that organisms use A/PCP pairs to partition an amino acid into secondary metabolism.

Introduction

Pyrrole moieties are found in a number of structurally diverse natural products that have a wide range of biological activities. Two coumarin group antibiotics, coumermycin A_1 and chlorobiocin (Figure 1), each contain a 5-methyl-pyrrolyl-2-carboxyl group at the C-3′ position of the noviose sugar. In addition to having two 5-methyl-pyrrolyl-2-carboxyl substituted noviose sugars, coumermycin A_1 also contains a 3-methyl-2,4-dicarboxyl pyrrole linker at its center. Both of these coumarin group antibiotics exert their activity by inhibiting type II DNA topoismerase DNA gyrase [1, 2]. The antifungal compounds pyrrolnitrin and pyoluteorin (Figure 1) each contain chlorinated pyrrole moieties. Pyrrolnitrin is a 3-chloro-4-(2′-nitro-3′-chlorophenyl)-pyrrole that is believed to play an important role in the biocontrol properties of *Pseudomonas* strains [3, 4]. Pyoluteorin, which enhances biocontrol activity of *Pseudomonas fluorescens* strains [5], contains a 4,5-dichloro-pyrrolyl-2-carboxyl linked to a resorcinol ring. Finally, members of the prodigiosin group of red pigments are unusual in having a tripyrrole structure and possess anticancer [6], antimicrobial [7], and promising immunosuppressive activities [8]. Two examples of these compounds are undecylprodigiosin from *Streptomyces coelicolor* A3(2) and prodigiosin from *Serratia marcescens* (Figure 1).

The most thoroughly studied mechanism for pyrrole biosynthesis is the generation of porphobilinogen, an early intermediate in porphyrin and corrin ring synthesis, by the condensation of two molecules of δ-aminolevulinate by δ-aminolevulinate dehydratase (Figure 2A) [9]. Evidence for an alternative pathway for pyrrole synthesis comes from intermediate accumulation and feeding experiments for pyrrolnitrin biosynthesis in *P. fluorescens* [3]. In that study, the accumulation of 7-chlorotryptophan (Figure 2B) in a Δ*prnB* strain of *P. fluorescens* and the restoration of pyrrolnitrin synthesis in this strain by the addition of exogenous monodechloroaminpyrrolnitrin or other downstream intermediates strongly suggests that PrnB catalyzes the rearrangement of the 7-chlorotryptophan indole ring to a phenylpyrrole and its decarboxylation to generate monodechloroaminpyrrolnitrin (Figure 2B). Mechanistic studies on PrnB have yet to be performed. The pyrrole moiety of the indole ring of L-tryptophan itself is catalyzed by indole-3-glycerol phosphate synthase (Figure 2C; [10]). A new mechanism for pyrrole synthesis has been suggested from precursor labeling studies on the biosynthesis of pyoluteorin [5], coumermycin A_1 [11], undecylprodigiosin [12], and prodigiosin [13]. These labeling studies found that L-proline was the precursor for the pyrrole moieties in pyoluteorin and coumermycin A_1 and for pyrrole ring (a) of the prodigiosins. This would imply a pyrrole biosynthetic pathway distinct from the previously characterized mechanisms discussed above.

The recent sequencing of the biosynthetic gene clusters for pyoluteorin [5], undecylprodigiosin [14], and coumermycin A_1 [15] gave a chance to elucidate the possible mechanism for the conversion of the pyrrolidine ring of L-proline to a pyrrole (Figure 2D). It should be noted that although *S. coelicolor* A3(2) produces a mixture of prodigiosins, it is presumed that they all share the same pathway for the biosynthesis of the tripyrrole core [7]. Sequence homology with adenylation (A) domains of nonribosomal peptide synthetases (NRPSs) suggests that PltF (pyoluteorin), SC3F7.11 (undecylprodigiosin), and ProC (coumermycin A_1) function as amino acid-activating enzymes. These domains in NRPSs activate their respective amino acid to aminoacyl-AMP intermediates, which are subsequently attacked by the thiol moiety of a 4′-phosphopantheine attached to a peptidyl carrier protein (PCP) to generate the aminoacyl-*S*-PCP intermediate. The following homologs of PCP domains also can be found in each cluster: PltL (pyoluteorin), SC3F7.09 (undecylprodigiosin), and ProB (coumermycin A_1). The combined activity of these A/PCP pairs would result in the formation of an L-prolyl-*S*-PCP intermediate. The subsequent oxidation of the covalently tethered intermediate is most likely catalyzed by enzymes showing homology with acyl-CoA dehydrogenases. These enzymes include PltE (pyoluteorin), SC2E9.21 (undecylprodigiosin), and ProC (coumermycin A_1). These dehydrogenases could func-

[1]Correspondence: christopher_walsh@hms.harvard.edu

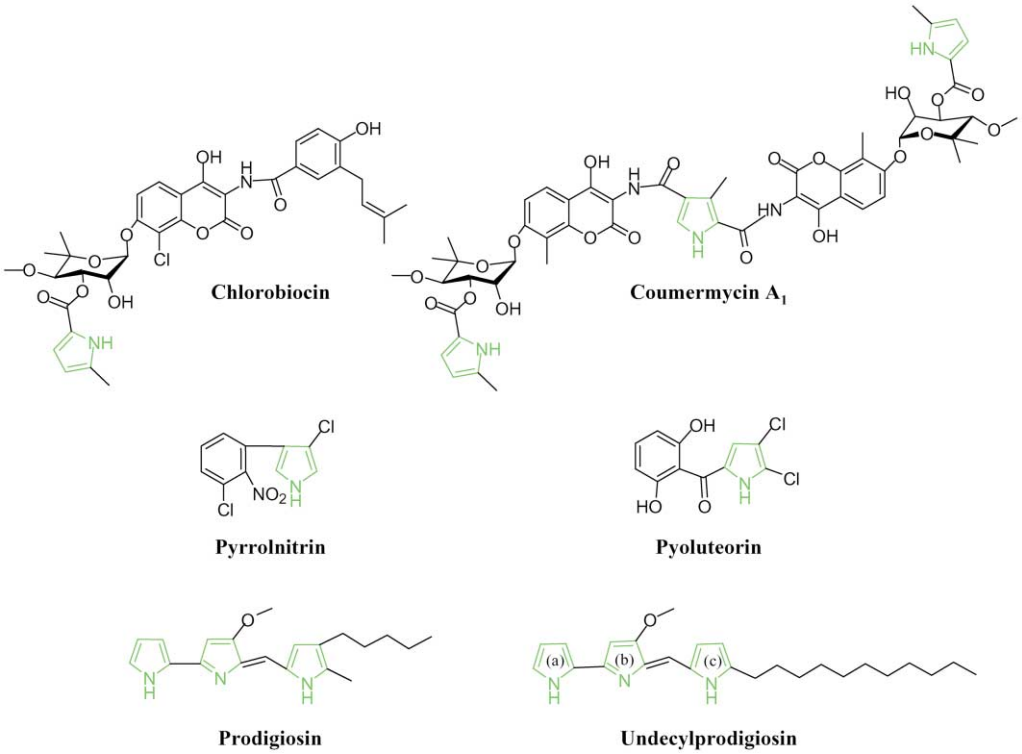

Figure 1. Chemical Structures of pyrrole-Containing Natural Products from Various Bacteria

The pyrrole moieties are highlighted in green, and the tripyrrole structure of undecylprodigiosin is labeled with pyrrole rings (a), (b), and (c) for reference throughout the text.

tion to oxidize both sides of the proline ring or, alternatively, to form the Δ^2-pyrrolinyl-2-carboxyl-*S*-PCP intermediate, which spontaneously air oxidizes to the pyrrolyl-2-carboxyl-*S*-PCP [5]. In the case of pyoluteorin, the pyrrolyl-2-carboxyl-*S*-PCP intermediate would subsequently be transferred to the pyoluteorin polyketide synthase either before or after chlorination. It is not clear how the pyrrolyl moiety is attached to the noviose sugar in coumermycin A_1 [15]. We are currently studying how pyrrole ring (a) from undecylprodigiosin is incorporated into the final product. The prediction outlined above for pyrrole synthesis during undecylprodigiosin, pyoluteorin, and coumermycin A_1 biosynthesis has yet to be proven biochemically.

Here we present the biochemical characterization of pyrrolyl-2-carboxyl-*S*-PCP synthesis by both the pyoluteorin system outlined above (PltF, PltE, and PltL) and the homologous system uncovered by the ongoing *S. coelicolor* A3(2) sequencing project [14] for the undecylprodigiosin biosynthetic cluster (SC3F7.11, SC3F7.09, and SC2E9.21). In both systems we show how these three proteins work in unison to generate pyrrole moieties by a mechanism not previously seen for pyrrole synthesis.

Results

Characterization of SC3F7.11 and PltF as L-prolyl-AMP Ligases

PltF, from the *P. fluorescens* Pf-5 pyoluteorin biosynthetic cluster, showed amino acid sequence homology (38% identity and 50% similarity) with an ORF (SC3F7.11, referred to here on as ORF11) from *S. coelicolor* A3(2). The genome for this strain of *S. coelicolor* is currently being sequenced, and ORF11 is encoded within a region of the genome previously shown to be involved in the biosynthesis of the tripyrrolic compound undecylprodigiosin [16, 17]. Analysis of the protein sequence of ORF11 and PltF revealed that they were homologous to A domains of NRPSs. During NRPS-catalyzed peptide synthesis, A domains function as aminoacyl-AMP ligases and generate the corresponding aminoacyl-AMP intermediate, by using ATP as a cosubstrate, then catalyze the subsequent transfer of the activated amino acid to the 4′-phosphopantetheinyl prosthetic group of a partner holo-PCP [18, 19]. Based on the structures of undecylprodigiosin and pyoluteorin, it was anticipated that ORF11 and PltF would function as L-prolyl-AMP ligases. Two recent studies have proposed that the amino acid substrate specificity of an A domain can be determined by sequence analysis of the amino acid residues presumed to surround the substrate binding pocket [20, 21]. Analysis of the corresponding residues from ORF11, PltF, and ProC (coumermycin A_1) sequences (DL[F/L]YLALVCK according to the Stachelhaus et al. rules [20]) did not predict that these enzymes would contain the expected proline-specific binding pocket. This suggested that these enzymes, if they did activate proline, would fall into a separate proline-activating cluster.

To determine if ORF11 and PltF were, in fact, L-prolyl-AMP ligases, we PCR amplified the genes encoding

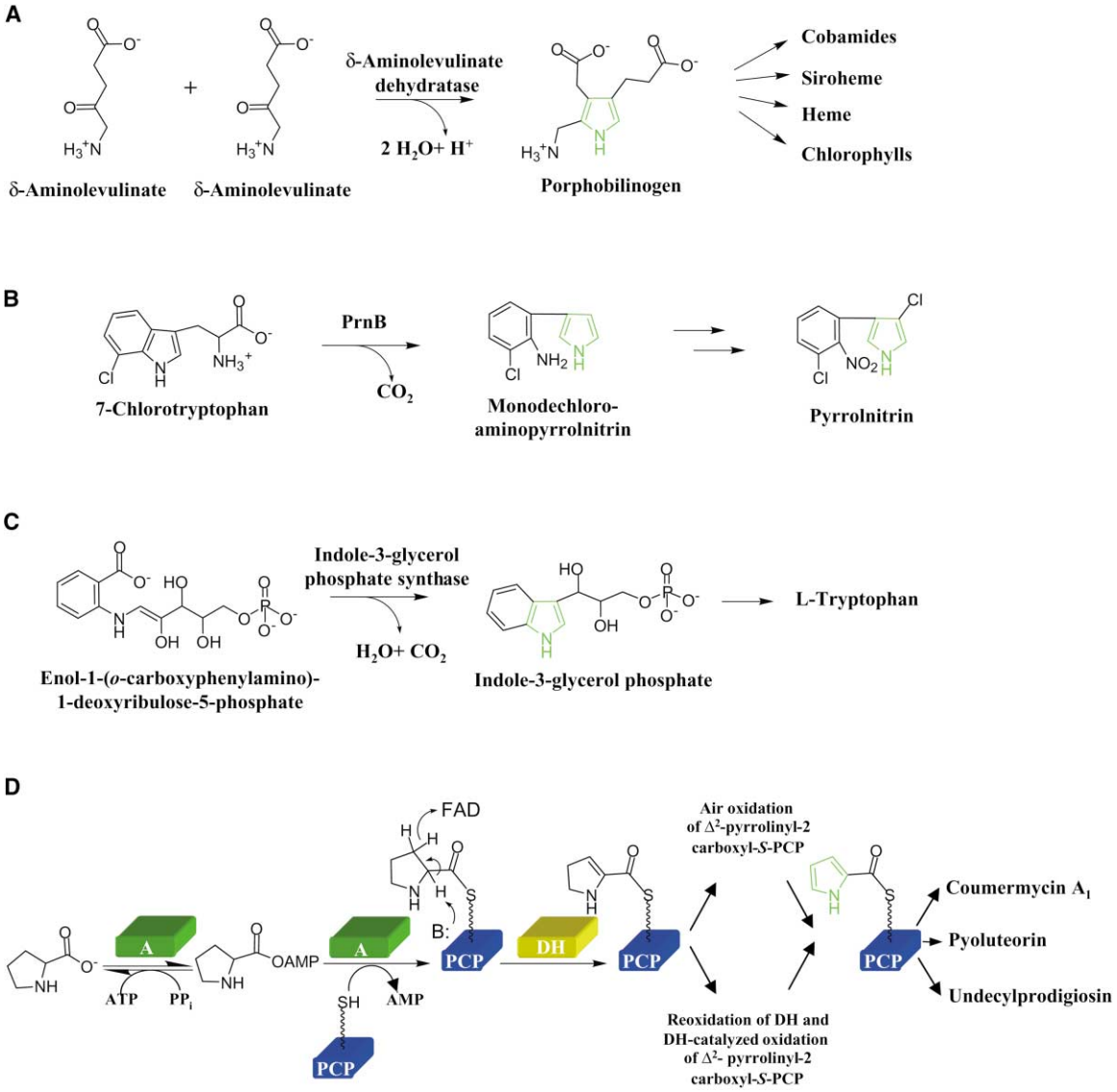

Figure 2. Schematic Representation of Known Mechanisms for Pyrrole Biosynthesis

(A) Substrates and products of the reaction catalyzed by δ-aminolevulinate dehydratase to generate porphobilinogen, an intermediate of porphorin and corrin ring biosynthesis.

(B) Substrate and products for the proposed PrnB-catalyzed reaction during pyrrolnitrin biosynthesis.

(C) Substrate and products of the reaction catalyzed by indole-3-glycerol phosphate synthase, an enzyme involved in tryptophan biosynthesis.

(D) A schematic representation of pyrrolyl-2-carboxyl-*S*-PCP synthesis based on amino acid sequence analysis of ORFs encoded within the undecylprodigiosin, pyoluteorin, and coumermycin A_1 biosynthetic pathways. L-prolyl-AMP ligase (adenylation, A) is green, the peptidyl carrier protein (PCP) is blue, and the acyl-CoA dehydrogenase (DH) homolog is yellow. In all reactions, the pyrrole moiety of the product is highlighted in green.

each of the enzymes and cloned them into the T7 overexpression vector pET37b. These constructs resulted in the expression of enzymes with C-terminal His8 tags for nickel affinity chromatography. Each enzyme was overexpressed in *E. coli* BL21(DE3) and purified by nickel affinity chromatography followed by Q Sepharose ion exchange chromatography. These two purification steps resulted in ORF11 and PltF being purified to near homogeneity based on SDS-PAGE and Coomassie blue staining (Figure 3A).

The classic method for analyzing A domains of NRPSs for aminoacyl-AMP formation and substrate specificity is by monitoring substrate-dependent ATP-[^{32}P]PP_i exchange reactions, an assay initially developed for analyzing tRNA synthetases [22]. Using this end-point assay, we tested the substrate specificity of each enzyme by using the following substrates: L-proline, pyrrolyl-2-carboxylate, D-proline, glycine, and L-serine. L-proline was the favored substrate for both ORF11 and PltF, with only very low levels of D-proline and glycine activation (Figure 3B). The kinetic parameters for L-proline activation by ORF11 and PltF (Table 1) were typical for A domains of NRPSs [23–26], giving further support for L-proline as the natural substrate.

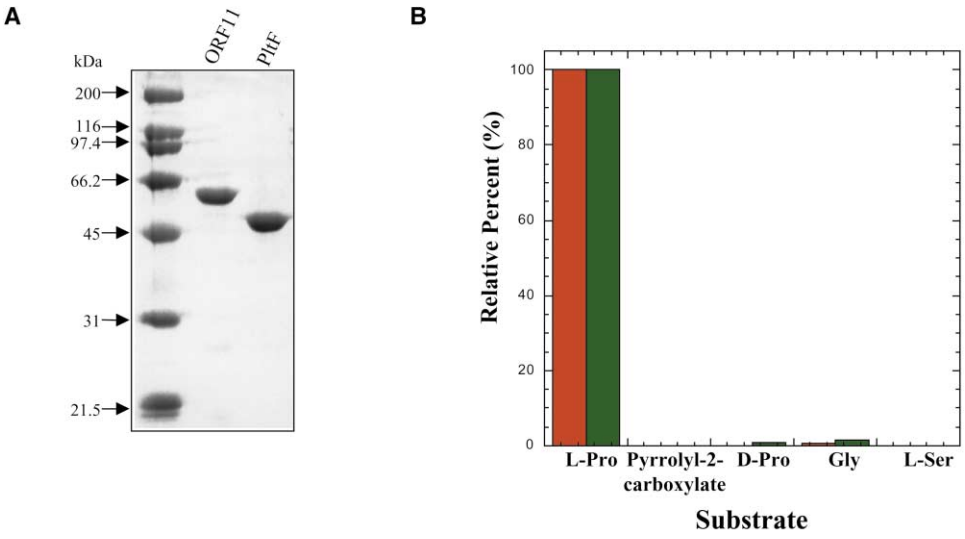

Figure 3. Purification and Substrate Specificity of ORF11 and PltF

(A) Coomassie-stained 12% SDS-PAGE gel showing purified ORF11 and PltF proteins. Protein (1.5 μg) was loaded in each lane.

(B) Relative activity of substrate-dependent ATP-[^{32}P]PP$_i$ exchange catalyzed by ORF11 (red) and PltF (green). Data are representative 10 min end-point assays.

Based on these results, a few conclusions could be drawn about undecylprodigiosin and pyoluteorin biosynthesis. The fact that ORF11 was specific for L-proline in combination with the prior observation that L-proline is incorporated into only pyrrole ring (a) of the tripyrrole [12] suggests ORF11 is likely involved in the synthesis of this particular pyrrole ring of undecylprodigiosin. Furthermore, neither glycine nor L-serine, the two other amino acids incorporated into rings (b) and (c) of undecylprodigiosin, respectively [12], was a substrate for ORF11, and this finding lends further support for the above conclusion. Additionally, since pyrrolyl-2-carboxylate was not activated by either ORF11 or PltF, it could be concluded that oxidation of L-proline to the pyrrole must occur downstream of L-prolyl-AMP formation and not on the free amino acid. Finally, the oxidation of proline is likely to be stereospecific in both pathways since neither enzyme activated D-proline to a significant extent. Based on all of these results, it could be concluded that ORF11 and PltF were L-prolyl-AMP ligases.

Characterization of SC3F7.09 and PltL as Peptidyl Carrier Proteins (PCPs)

During NRPS-catalyzed peptide synthesis, the activation of each amino acid substituent involves two steps. The first step is the generation of the aminoacyl-AMP intermediate by the A domain, then the thioesterification of the amino acid to the 4′-phosphopantetheinyl prosthetic group of the partner holo-PCP domain to form an aminoacyl-*S*-PCP intermediate [18, 19]. SC3F7.09 (referred to here on as ORF9) of the undecylprodigiosin cluster and PltL from pyoluteorin are annotated in both biosynthetic clusters as hypothetical proteins because they do not show strong amino acid homology with any proteins in the public data bank, with the exception of ProB of the coumermycin A$_1$ biosynthetic cluster [15]. However, these ORFs do show weak homology (PSI-BLAST scores of ≤31) with putative PCP domains from a few antibiotic biosynthetic clusters known to be synthesized in an NRPS-dependent manner. It has been proposed that PltL [5] and ProB, from the coumermycin A$_1$ biosynthetic pathway [15], are possible acyl carrier proteins (ACPs) involved in pyrrole synthesis for their respective systems. ACPs are found in polyketide synthases and are analogous to PCP domains [27]. Although ORF9 and PltL appeared to contain the required serine residue that is posttranslationally modified with a 4′-phosphopantetheinyl prosthetic group, neither ORF showed the canonical flanking sequence of typical PCP, ACP, or related aryl carrier proteins (ArCP) [28].

Table 1. Kinetic Parameters for ORF11 and PltF L-Proline-Dependent ATP-[^{32}P]PP$_i$ Exchange

Enzyme	K_m (mM)	k_{cat} (min^{-1})
ORF11	1.54 ± 0.17	170.9 ± 7.8
PltF	0.51 ± 0.04	332.6 ± 8.4

4′-Phosphopantetheinylation of ORF9 and PltL

To test whether ORF9 and PltL were the PCP partners for ORF11 and PltF, respectively, we PCR amplified the gene encoding each protein and cloned it into a pET expression vector. Each construct resulted in the expression of a C-terminally His6-tagged protein. Each protein was overexpressed in *E. coli* BL21(DE3) with or without the coexpression of Sfp, a nonspecific 4′-phosphopantetheinyltransferase (PPTase) from *Bacillus subtilis* [29]. PCP proteins must be posttranslationally modified with a 4′-phosphopantetheinyl prosthetic group to generate functional holo-PCP [30], and often, overexpressed heterologous PCP, ACP, or ArCP domains in *E. coli* are not fully modified by the endogenous PPTases of *E. coli* [31, 32]. Overexpression of carrier proteins in the presence of Sfp usually results in

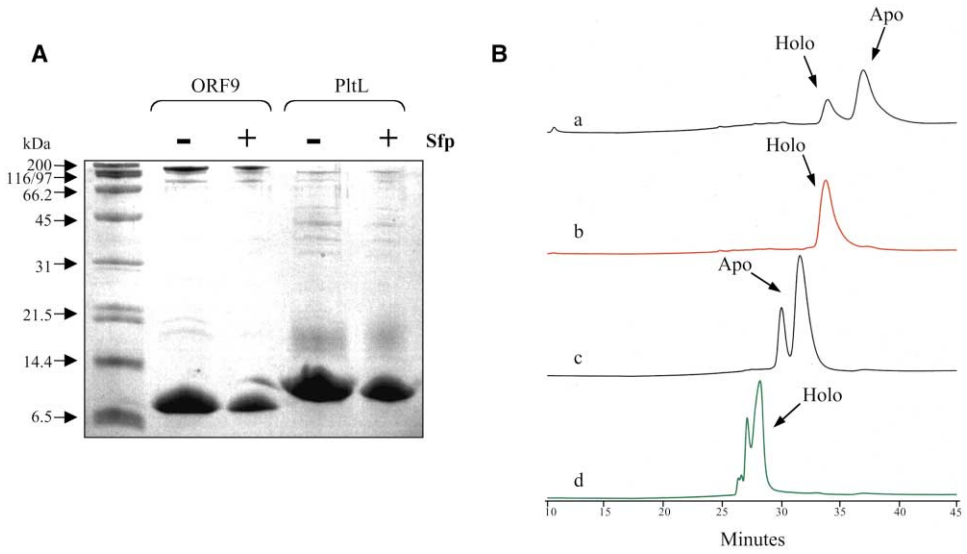

Figure 4. Purification and HPLC Analysis of ORF9 and PltL

(A) Coomassie-stained 16% SDS-PAGE Tris-Tricine gel of purified ORF9 and PltL protein expressed in the absence or presence of Sfp. Seventy-five micrograms of ORF9 and PltL expressed without Sfp were loaded, while 36 μg of ORF9 and PltL expressed with Sfp were loaded. (B) HPLC separation of ORF9 and PltL expressed in the absence or presence of Sfp. Trace a shows ORF9 without Sfp coexpression. Trace b (red) shows ORF9 with Sfp coexpression. Trace c shows PltL without Sfp coexpression. Trace d (green) shows PltL with Sfp coexpression.

fully modified protein. After overexpression of ORF9 and PltL in the presence or absence of Sfp coexpression, each protein was purified via nickel affinity chromatography followed by Q Sepharose ion exchange chromatography (Figure 4A).

To determine the extent of ORF9 and PltF 4′-phosphopantetheinylation, we analyzed each of the purified proteins by HPLC (Figure 4B) and MALDI-TOF MS (Table 2). By HPLC analysis, ORF9 was only 25% holo-PCP versus 75% apo-PCP in the absence of Sfp coexpression (Figure 4B, trace a), but it was >95% holo-PCP when coexpressed with Sfp (Figure 4B, trace b). This result was supported by MALDI-TOF MS analysis, where the difference in the mass of ORF9 with or without Sfp coexpression was as expected for 4′-phosphopantetheinyl modification (Table 2). HPLC analysis indicated that PltF was approximately 100% apo-PCP in the absence of Sfp (Figure 4B, trace c) but that it was approximately 100% holo-PCP in the presence of Sfp coexpression (Figure 4B, trace d), and total conversion was confirmed by MALDI-TOF MS analysis of the two proteins (Table 2). Further support for fully modified ORF9 and PltF will be discussed below. It was not clear why holo- and apo-PltL eluted from the HPLC as two peaks.

Table 2. MALDI-TOF MS Data Demonstrating the 4′ Phosphopantetheinylation of PCPs

PCP (+/− Sfp coexpression)	Calculated (Da)	Observed (Da)
ORF9	11,049	11,050[a]
ORF9 + Sfp	11,388	11,391[a]
PltL	11,872	11,873[b]
PltL + Sfp	12,211	12,245[b]

[a] Represents the average of two results.
[b] Represents the average of three results.

Aminoacylation of Holo-PCPs by Their Respective L-prolyl-AMP Ligases

To determine whether holo-ORF9 and holo-PltL are aminoacylated by ORF11 and PltF, respectively, we incubated the two protein pairs (ORF9/ORF11 and PltL/PltF) independently with [^{14}C]-L-proline and ATP and monitored aminoacylation of the holo-PCPs by standard TCA precipitation and scintillation counting [24, 26, 33]. In parallel reactions, we incubated each holo-PCP with the noncognate L-prolyl-AMP ligase to determine if the aminoacylation reaction required specific protein/protein interactions. This analysis demonstrated that holo-ORF9 and holo-PltL were aminoacylated by their respective L-prolyl-AMP ligases (Figure 5). Furthermore, both PCP proteins were fully aminoacylated in approximately 30 min, giving further support for complete 4′-phosphopantetheinylation of each PCP by Sfp during coexpression. The failure to detect aminoacylation of the holo-PCP domains with the noncognate L-prolyl-AMP ligase suggested that specific protein/protein interactions were required for successful aminoacylation. The kinetic parameters of holo-PCP aminoacylation were determined (Table 3), and these parameters, with a K_ms of about 10 μM and a k_{cat}s of about 1 s^{-1}, were similar to those observed in NRPS systems where the aminoacyl-AMP ligase must aminoacylate the cognate holo-PCP in trans [34, 35]. The successive steps of L-prolyl-AMP formation followed by thioesterification of the amino acid to the holo-PCP domain sets the stage for the next step in the biosynthetic pathways, the oxidation of the L-prolyl-*S*-PCP to pyrrolyl-2-carboxyl-*S*-PCP.

Characterization of SC2E9.20 (RedW) and PltE as L-prolyl-*S*-PCP Dehydrogenases

SC2E9.20 and PltE show strong amino acid homology with members of the acyl-CoA dehydrogenase/oxidase

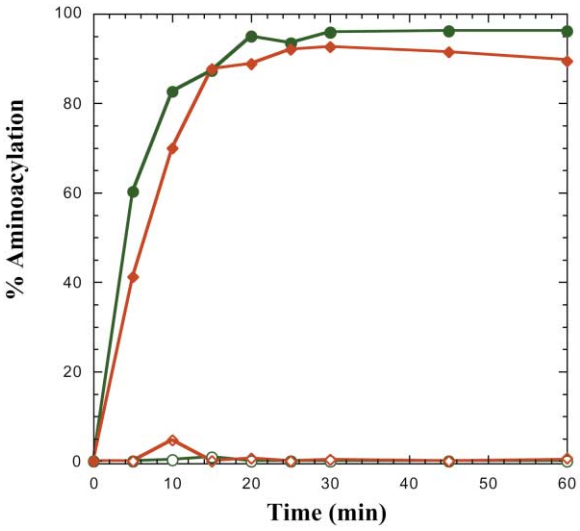

Figure 5. Representative Time Course of L-prolyl-AMP Ligase-Catalyzed Aminoacylation of Holo-PCPs by the Use of [^{14}C]L-Proline

Radiolabeled substrate incorporation was monitored by TCA precipitation of the proteins and subsequent liquid scintillation counting. See Experimental Procedures for details. Solid red circles represent a ORF9/ORF11 pair. Open red circles represent a ORF9/PltF pair. Solid green diamonds represent a PltL/PltF pair. Open green diamonds represent a PltL/ORF11 pair.

superfamily and show 45% identity and 58% similarity with each other. Additionally, ProA from the coumermycin A_1 biosynthetic cluster has a high degree of sequence homology with SC2E9.20 (PSI-BLAST score = 213). SC2E9.20 is referred to as RedW in the annotated sequence because of its probable role in the synthesis of undecylprodigiosin, a red pigment [36]. Acyl-CoA dehydrogenases/oxidases are flavoenzymes that catalyze double bond formation between the C-2 and C-3 of their thioester substrates [37]. It was intriguing to speculate that RedW and PltE react not with the coenzyme A thioester of L-proline (L-prolyl-*S*-CoA) but rather with the L-prolyl group thioesterified to the respective holo-PCP domain. Both enzymes would probably catalyze the formation of a Δ^2-pyrrolinyl-2-carboxyl-*S*-PCP intermediate; subsequent two-electron oxidation to pyrrolyl-2-carboxyl-*S*-PCP could occur by either of the two routes summarized in Figure 2C.

Overexpression and Purification of RedW and PltE from E. coli

The genes encoding RedW and PltE were PCR amplified and cloned into the overexpression vector pET37b.

Table 3. Kinetic Parameters for ORF11 and PltF Aminoacylation of Their Cognate PCP

L-prolyl-AMP ligase	PCP substrate	K_m (μM)	k_{cat} (min^{-1})[a]
ORF11	holo-ORF9	8.3 ± 1.9	40.5 ± 6.1
PltF	holo-PltL	10.2 ± 0.9	70.7 ± 2.0

[a] Values represent the minimum k_{cat} due to the inability to saturate the L-prolyl-AMP ligase with L-proline because of the detection limits of the assay. L-proline was 0.5 times the K_m for ORF11 and 1.5 times the K_m for PltF.

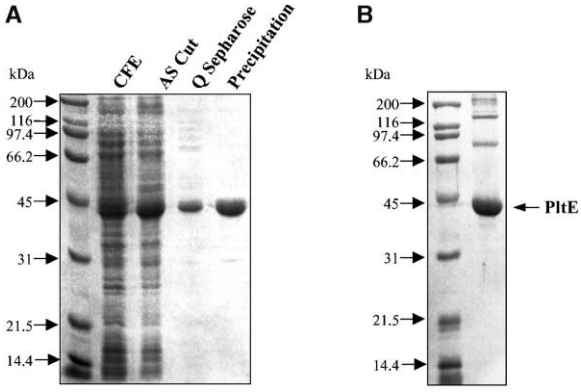

Figure 6. Purification of RedW and PltE

(A) Coomassie-stained 12% SDS-PAGE gel of samples from each step in RedW purification. Purified RedW (1.5 μg) is loaded in the precipitation lane.

(B) Coomassie-stained 12% SDS-PAGE gel of PltE purified by nickel chelate chromatography. PltE (5.5 μg) was loaded.

These constructs resulted in the expression of fusion proteins containing a C-terminal His8 tag for initial attempts to purify the enzymes via nickel affinity chromatography. Both constructs were overexpressed in *E. coli* BL21(DE3) strains, and initial attempts to purify the enzymes via His•Bind (Novagen) nickel affinity chromatography were unsuccessful because both enzymes precipitated out of solution when resin was added to cell-free extract. Thus, alternative purification procedures had to be developed.

RedW was determined to be insoluble when the NaCl concentration of the buffer was below 300 mM or the glycerol concentration was below 10% (v/v). With this in mind, the following purification procedure was developed for enzyme. First, ammonium sulfate precipitation was performed on the cell-free extract, and RedW was found to precipitate between 20% and 40% (saturated) ammonium sulfate. The second step involved Q Sepharose ion exchange chromatography, for which the enzyme was diluted to a final NaCl concentration of 100 mM immediately prior to being loaded onto the column. This procedure minimized precipitation of the protein prior to its binding to the Q Sepharose column, and the protein could be eluted with a linear NaCl gradient. The final purification step took advantage of the protein precipitating when the NaCl concentration was below 300 mM. RedW that had eluted from the Q Sepharose column was dialyzed overnight against buffer containing only 100 mM NaCl. During this dialysis, the protein precipitated and could be recovered by centrifugation. After removal of the supernatant, the precipitated enzyme could be resolubilized in buffer containing 300 mM NaCl, and activity was retained. This purification protocol resulted in protein that was purified to near homogeneity based on SDS-PAGE and Coomassie blue staining (Figure 6A). An alternative final step of size exclusion chromatography also resulted in functional, pure protein (our unpublished data). Analysis of the protein by UV-Vis spectroscopy and HPLC analysis showed that the flavin was retained during the purification procedure (Figure 7A) and that this flavin was FAD (Figure 7B), as expected

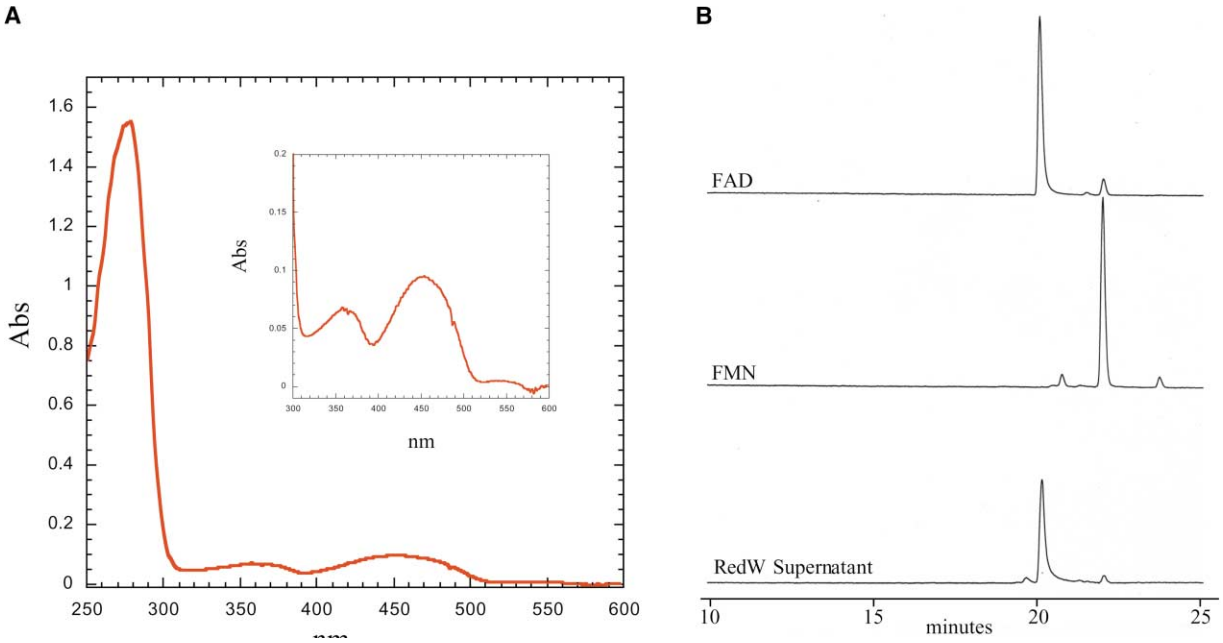

Figure 7. UV-visible spectrum of RedW and HPLC Analysis of the Flavin Cofactor of RedW

(A) UV-visible spectrum of purified RedW protein. The spectrum highlights the λ_{max} at 350 and 450 nm. The spectrum shown is for 70 μM RedW.

(B) HPLC separation and identification of FAD as the cofactor of RedW. FAD and FMN standards eluted with retention times of 20.3 and 22.2 min, respectively. RedW was boiled for 5 min, protein was removed by centrifugation, and the supernatant was recovered and used for HPLC analysis. The RedW flavin eluted with a retention time of 20.3 min, consistent with the cofactor being FAD. Coinjection of authentic FAD and RedW supernatant resulted in coelution of the flavins at 20.3 min (our unpublished data).

for members of the acyl-CoA dehydrogenase/oxidase family [37].

PltE could be purified by nickel affinity chromatography when Ni-NTA Superflow (Qiagen) resin was used instead of His•Bind. PltE could be partially purified by this purification procedure (Figure 6B); however, a majority of the enzyme lacked the bound flavin cofactor. The inclusion of excess FAD in the buffer during sonication and batch binding to the resin resulted in the elution of holo-enzyme; however, the FAD was lost after overnight dialysis in the absence of excess FAD. Further purification of the enzyme was not successful because of the instability of the enzyme. Therefore, PltE was characterized in the partially purified form shown in Figure 6B. Based on the results with RedW, it was assumed that FAD was the natural cofactor. Thus, to compensate for the loss of cofactor during dialysis, we performed the analysis of PltE-catalyzed pyrrolyl-2-carboxyl-*S*-PltL formation in the presence of excess FAD.

Substrate-Dependent FAD Reduction

Acyl-CoA dehydrogenases catalyze substrate oxidation via hydride transfer from the substrate to the FAD cofactor and then by product release contingent upon $FADH_2$ reoxidation [37]. This process can be monitored spectrophotometrically by following the characteristic decrease in the flavin absorbance at 350 and 450 nm upon reduction. This could not be monitored for PltE because of the requirement for excess FAD to be added to the reactions. RedW, however, did not have this requirement and was used for detecting substrate-dependent hydride transfer. The assays were performed aerobically, and the reduction of the FAD cofactor was observed (Figure 8). This reduction required L-proline, ATP, holo-ORF9, ORF11, and RedW (our unpublished data) and suggested that L-prolyl-*S*-PCP oxidation had occurred. The level of FAD reduction also varied with holo-ORF9 concentrations as would be expected (Figure 8). The replacement of ORF9 and ORF11 with the complementary PltL/PltF pair did not result in FAD reduction (our unpublished data), suggesting that specific protein/protein interactions were important for efficient catalysis. Taking approximately 20 min after full FAD reduction, the aerobic reoxidation of the $FADH_2$ was slow and suggested that RedW was a dehydrogenase, not an oxidase. This aspect of RedW and PltE is discussed in further detail below.

Analysis of the RedW and PltE Reaction Products

RedW and PltE catalysis is expected to generate the conjugated Δ^2-pyrrolinyl-2-carboxyl-*S*-PCP, and subsequent air oxidation should generate the Δ^4-ene in the pyrrolyl($\Delta^{2,4}$-diene)-2-carboxyl product as previously proposed [5, 15]. Thus, the product of complete reactions (L-proline, ATP, L-prolyl-AMP ligase, PCP, and the putative L-prolyl-*S*-PCP dehydrogenase) for both systems may be pyrrolyl-2-carboxyl-*S*-PCP. To simplify the characterization of the reaction products, we hydrolyzed the covalently bound products from the PCP by brief heating in 0.1 M KOH after TCA precipitation and removal of unbound components. After hydrolysis, the products were separated by HPLC (Figure 9). Both RedW- and PltE-containing reactions produced a product that had the same retention time as authentic pyrro-

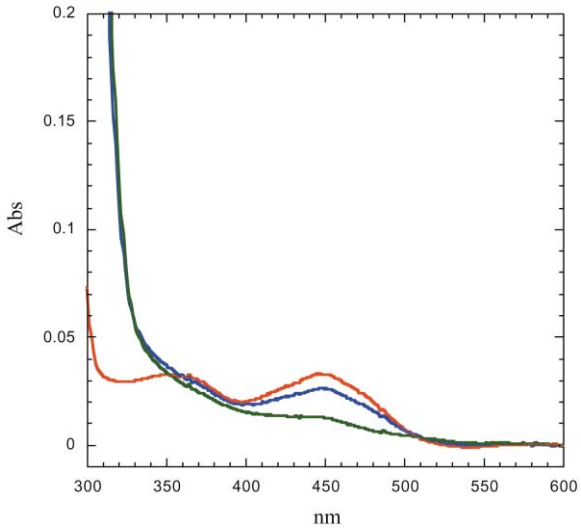

Figure 8. UV-Visible Spectrum of RedW Flavin Reduction by L-prolyl-*S*-ORF09

The Red trace is the spectrum of 10 μM RedW in a reaction mixture containing 100 nM ORF11, 30 μM holo-ORF9, and 5 mM ATP prior to the addition of L-proline, which brought the mixture to a final concentration of 10 mM. The green trace is the spectrum of RedW 10 min after L-proline addition. The blue trace is the same reaction conditions except that the holo-ORF9 concentration was lowered to 15 μM; again, the spectrum was taken 10 min after L-proline addition.

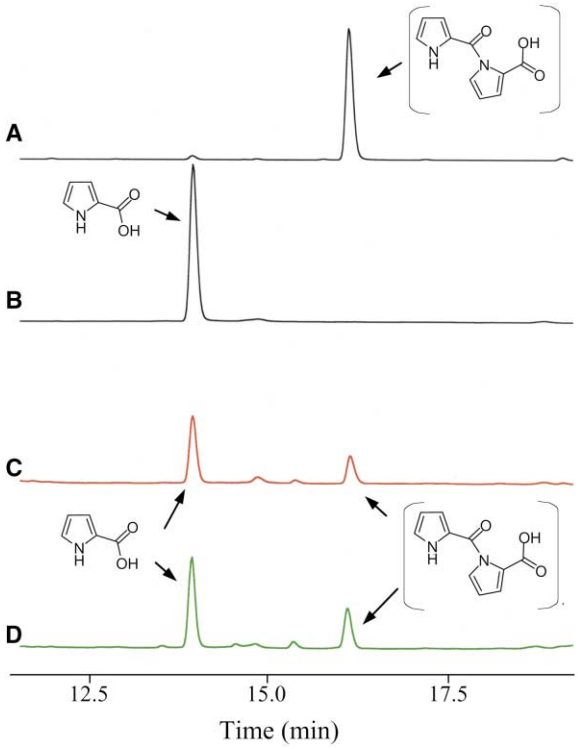

Figure 9.

HPLC separation and identification of ORF11/ORF9/RedW (Red) and PltF/PltL/PltE (green) reaction products released by KOH treatment. See Experimental Procedures for details. Trace a shows pyrrolyl-2-carboxyl-SNAC after KOH treatment. Trace b shows authentic pyrrolyl-2-carboxylate. Trace c shows ORF11/ORF9/RedW reaction products. Trace d shows PltF/PltL/PltE reaction products. Chemical structures of the eluted compounds are shown. The putative bipyrrole structure is shown in brackets.

lyl-2-carboxylate, the expected hydrolysis product (Figure 9, traces c,d), regardless of the elution conditions. When the reaction mixture was coinjected with authentic pyrrolyl-2-carboxylate, both the authentic standard and the major hydrolysis product coeluted regardless of the elution conditions (our unpublished data). Additionally, this product had a UV-Vis spectrum indicative of pyrrolyl-2-carboxylate. Although the detection of pyrrolyl-2-carboxylate by mass spectrometry has been reported [38], we were unable to detect the mass of this product by using a variety of MS techniques (MALDI-TOF, ESI, LC/MS, CI, EI, and FAB). Additionally, the mass of authentic pyrrolyl-2-carboxylate could not be detected with these techniques. Therefore, to prove the this product was pyrrolyl-2-carboxylate, we performed ^{1}H NMR on product from a scaled-up reaction. The chemical shift and coupling constants (^{1}H NMR [CD_3OD, 500 MHz] d 6.18 [dd, 1H, J = 3.4, 2.4 Hz], 6.84 [dd, 1H, J = 3.6, 1.5 Hz], and 6.95 [dd, J = 2.4, 1.5 Hz, 1H]) of the purified product were in agreement with those from authentic pyrrolyl-2-carboxylate and published data [39].

An additional product peak, with an elution time of 16 min, was observed in both reactions (Figure 9). Repeating the RedW experiment with [^{14}C-L-Proline] showed that this second product was derived from proline (our unpublished data). During the work-up of the reactions, the products were hydrolyzed from the PCP domains by incubation at 65°C for 15 min in 0.1 M KOH. This treatment may have caused the formation of some adduct of pyrrolyl-2-carboxylate. To test this theory, we chemically synthesized a pyrrolyl-2-carboxyl-*N*-acetylcysteamine thioester (pyrrolyl-2-carboxyl-SNAC) product mimic (Figure 10). This product mimic was incubated at 65°C for 15 min in 0.1 M KOH, and the resulting products were separated by HPLC (Figure 9, trace a). A product peak eluting with the same retention time, regardless of changes in the elution profile, as the unidentified RedW and PltE product peak was observed, and it showed the same UV-Vis spectrum as the product eluting from the RedW and PltE reactions (our unpublished data). This product was not observed when authentic pyrrolyl-2-carboxylate was treated in the same manner and suggested that formation of this product required the thioesterfied pyrrolyl-2-carboxylate. Analysis of this product peak by a variety of mass spectrometry techniques (MALDI-TOF, LC/MS, ESI, CI, and EI) failed to detect a reliable mass to identify the product. The amount of product accumulated was not enough to solve the chemical structure by NMR. One explanation for this product formation was that in the presence of 0.1 M KOH, the nitrogen of the pyrrole ring became deprotonated and the resulting nucleophile attacked the carbonyl center of a neighboring pyrrolyl-2-carboxyl-*S*-PCP thioester, generating a bipyrrole adduct. Consistent with this model, an increase in the pyrrolyl-2-carboxyl-SNAC concentration could bias the ratio of pyrrolyl-2-carboxylate to the putative bipyrrole toward

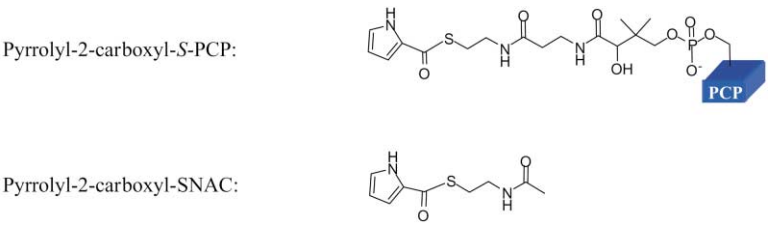

Figure 10. Schematic Representation of the Pyrrolyl-2-Carboxyl-*S*-PCP Product Compared to the Product Mimic Pyrrolyl-2-Carboxyl-SNAC

See Experimental Procedures for details on pyrrolyl-2-carboxyl-SNAC synthesis.

the bipyrrole. Figure 9 trace a shows the product generated when formation of the putative bipyrrole was optimized. A similar effect was seen when the pyrrolyl-2-carboxyl-*S*-PCP concentration was varied during KOH treatment (our unpublished data). Finally, it should be noted that RedW could not substitute for PltE in pyrrolyl-2-carboxyl-*S*-PltL formation, whereas PltE could only partially substitute for RedW in pyrrolyl-2-carboxyl-*S*-ORF9 formation. This suggests that specific protein/protein interactions play a role in pyrrolyl-2-carboxyl-*S*-PCP formation.

Discussion

The results reported here establish a new mechanism for the biosynthesis of pyrrole moieties. The two pathways that were investigated are involved in the biosynthesis of the natural products undecylprodigiosin, from *S. coelicolor* A3(2), and pyoluteorin, from *P. fluorescens* Pf-5. In each pathway, an enzyme showing amino acid sequence homology with A domains of NRPSs (ORF11, undecylprodigiosin; PltF, pyoluteorin) is specific for L-proline activation to L-prolyl-AMP. This intermediate is subsequently thioesterified in trans to a partner protein showing homology to PCP domains of NRPSs (ORF9, undecylprodigiosin; PltL, pyoluteorin). The aminoacylation of the holo-PCP is followed by the oxidation of the L-prolyl-*S*-PCP to the corresponding pyrrolyl-2-carboxyl-*S*-PCP, a conversion initiated by a novel enzyme showing homology to acyl-CoA dehydrogenases/oxidases (RedW, undecylprodigiosin; PltE, pyoluteorin). In both biosynthetic pathways we show that the corresponding three-enzyme assemblage is sufficient for the conversion of the pyrrolidine ring of L-proline to a pyrrole.

The final enzymatic step in pyrrole synthesis is catalyzed by either RedW (undecylprodigiosin) or PltE (pyoluteorin), both of which show strong homology to members of the acyl-CoA-dehydrogenase/oxidase superfamily. The distinction between the enzyme functioning as a dehydrogenase or as an oxidase is based on whether $FADH_2$ reoxidation is catalyzed by O_2 (oxidase) or a partner electron-transferring flavoprotein (dehydrogenase). Our finding that the FAD cofactor of RedW is reduced by L-prolyl-*S*-ORF9 with very slow reoxidation of the flavin in the presence of O_2 suggests RedW, and by analogy PltE, functions as a dehydrogenase, not an oxidase. In support of this conclusion, preliminary results monitoring pyrrolyl-2-carboxylate formation by RedW suggested that the enzyme performs a single catalytic turnover in the presence of O_2 but multiple turnovers in the presence of ferricinium salt, a commonly used surrogate electron acceptor for the study of acyl-CoA dehydrogenases [40] (our unpublished data). These data support the conclusion that RedW and PltL function as L-prolyl-*S*-PCP dehydrogenases.

This raises the question of what functions as the electron-transferring flavoprotein (ETF) in each system. There are no ORFs shared between the undecylprodigiosin and pyoluteorin biosynthetic clusters that would suggest a common ETF. An ORF in the undecylprodigiosin biosynthetic cluster (SC2E9.21, *redY*), which is transcribed immediately downstream of *redW*, shows weak homology to flavin oxidoreductases. However, the overexpression and purification of this putative enzyme and its inclusion in RedW reaction mixtures did not stimulate multiple RedW turnovers, nor did the purified protein contain the expected flavin cofactor (our unpublished data). It is possible that the ETF involved in the β oxidation of fatty acids can be recruited for the reoxidation of the bound flavin of RedW or PltE.

The RedW- and PltE-catalyzed conversion of L-prolyl-*S*-PCP to pyrrolyl-2-carboxyl-*S*-PCP can occur by two alternative two-step routes. One pathway is the formation of the Δ^2-pyrrolinyl-2-carboxyl-*S*-PCP by the dehydrogenase and the subsequent two-electron oxidation to the pyrrolyl-2-carboxyl-*S*-PCP by either of the two steps outlined in Figure 2C. Alternatively, the reaction could proceed via enzyme-catalyzed Δ^4-pyrrolinyl-2-carboxyl-*S*-PCP production first, followed by two-electron oxidation. Based on the known biochemistry of acyl-CoA dehydrogenase catalysis [37, 41, 42], it is assumed that Δ^2-pyrrolinyl-*S*-PCP is formed first, followed by air oxidation to pyrrolyl-2-carboxyl-*S*-PCP. This is based on an extensive number of studies that have lead to the prediction that all acyl-CoA dehydrogenases catalyze substrate oxidation by a similar mechanism [41]. The proposed catalytic mechanism for these enzymes involves the abstraction of the acidic proton from the α-carbon of the thioesterified substrate to generate an enolate-like transition state. Subsequent β-hydride expulsion to the FAD cofactor results in the enoyl-*S*-CoA product. By analogy, the product formed by RedW or PltE catalysis will be the Δ^2-pyrrolinyl-2-carboxyl-*S*-PCP, and the subsequent two-electron oxidation is nonenzymatic. Interestingly, amino acid alignments of RedW and PltE with two acyl-CoA dehydrogenases, the crystal structures of which have been solved (pig liver medium-chain acyl-CoA dehydrogenase [43, 44] and human branched-chain isovaleryl-CoA dehydrogenase [41]) suggest that the catalytic base of RedW and PltE will be located in a position similar to that seen for the branched-chain acyl-CoA dehydrogenase. Additionally, neither RedW nor PltE appears to have the conserved residues involved in the recognition of the adenosine moiety of CoA.

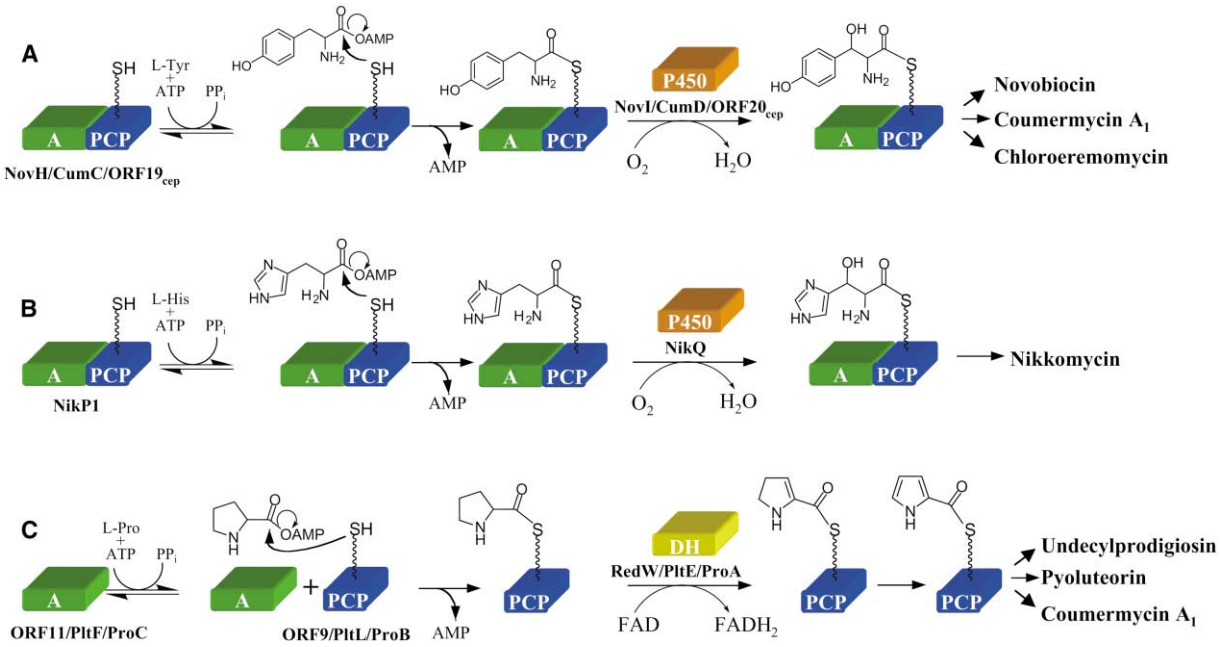

Figure 11. Schematic Representation of A/PCP-Catalyzed Amino Acid Thioesterification Followed by Downstream Modification by Partner Proteins

(A) Schematic of β-hydroxy-L-tyrosine biosynthesis as determined for novobiocin (NovH/I) biosynthesis (2). A similar mechanism is proposed for coumermycin A_1 (CumC/D) and chloroeremomycin ($ORF19_{cep}$/$ORF20_{cep}$) biosynthesis.

(B) Schematic of β-hydroxy-L-histidine biosynthesis as determined for nikkomycin (NikP1/NikQ) biosynthesis.

(C) Schematic of conversion of proline to pyrrolyl-2-carboxyl-*S*-PCP as determined for undecylprodigiosin (ORF11/ORF9/RedW) and pyoluteorin (PltF/PltL/PltE) and as proposed for coumermycin A_1 (ProC/ProB/ProA) biosynthesis. Analogous A and PCP domains/proteins are shown in green and blue, respectively. Downstream modification enzymes are shown in orange (P450 monooxygenases) or yellow (L-prolyl-*S*-PCP dehydrogenases).

It is important to highlight the specificity detected for protein/protein interactions in both pathways. We have shown that the aminoacylation of the holo-PCPs by their L-prolyl-AMP ligase partners is specific based on the finding that ORF11 could not aminoacylate holo-PltL, nor could PltF aminoacylate holo-ORF9. Furthermore, the kinetic parameters are consistent with correct protein/protein interactions since each pair shows $K_m \approx 10$ μM and k_{cat} 1 s^{-1}. This is important because both biosynthetic clusters encode multiple carrier protein homologs. In undecylprodigiosin, carrier protein homologs in addition to an autonomous ACP homolog are encoded within large multidomain proteins (our unpublished data). The pyoluteorin biosynthetic cluster encodes three ACP homologs found within two multidomain polyketide synthase proteins [5]. Our results showing specificity between L-prolyl-AMP ligase/PCP pairs would argue that the correct partner proteins have been identified. Further support for this conclusion comes from the finding that the L-prolyl-*S*-PCP dehydrogenases are also selective for their respective partner proteins. Finally, the PCPs characterized here show strong amino sequence homology to each other but not to other carrier protein homologs encoded by the remaining ORFs of the clusters. Thus, the correct PCP protein involved in the conversion of the pyrrolidine ring of proline to a pyrrole in each pathway was identified.

The modification of an amino acid thioesterified to a holo-PCP domain appears to be a common theme in secondary metabolism. Recently, it was shown that during novobiocin biosynthesis, the formation of β-hydroxyl-L-tyrosine is catalyzed by an A-PCP didomain protein (NovH) that covalently tethers L-tyrosine to its holo-PCP domain (Figure 11A). The L-tyrosinyl-*S*-

Table 4. Primers Used for the PCR Amplification of Undecylprodigiosin and Pyoluteorin Genes

Gene	5′ Primer	3′ Primer
SC3F7.09 (ORF9)	AGGACGCATATGACTCCTCGGAAACTG	CGGAGTAAGCTTTGCCGCGGTTCCCCC
SC3F7.11 (ORF11)	CTGTACCATATGAGCGCCGCCACTCCC	GTTCCGGGCAAGCTTCCGGGCCGTTCC
SC2E9.20 (*redW*)	CGCAACCATATGAACTTCGACTTCGAC	CTGACTGTGAAGCTTGCGGCGGGCCGC
pltL	TGTCATATGCAGGAGCGTACGTCT	TTTAGGCTCGAGGGCGCACTCGGCCTTTAG
pltF	GAACATATGAAGCTGCTCCATGAA	CATAAGCTTGCCCTCCACCTGCCTGGC
pltE	GTTCATATGGACTTCAACTACGAC	GCTGTGAAGCTTCCGTTCATGGAG

For each primer, the introduced restriction sites are underlined. For the 5′ primers, all introduced an NdeI restriction site. For the 3′ primers, all included HindIII sites except for *pltL*, which introduced an XhoI restriction site.

PCP is then hydroxylated by a partner cytochrome P450 monooxygenase (NovI) [45]. Based on sequence homology, it was proposed that this mechanism would be used to generate β-hydroxyl-L-tyrosine not only for novobiocin but also for coumermycin A_1 [15] and chloroeremomycin biosynthesis [45]. Additionally, it has been shown that the formation of β-hydroxyl-L-histidine during nikkomycin biosynthesis will be analogous based on the function of an A-PCP/P450 pair in the biosynthetic cluster (Figure 11B; [46]). The pyrrolyl-2-carboxyl-*S*-PCP biosynthetic pathways characterized here, and assumed to also occur during coumermycin A_1 biosynthesis, extend this theme (Figure 11C). The tethering of an amino acid onto a holo-PCP prior to downstream modification serves two roles. First, it diverts a portion of the cellular pools of an amino acid into secondary metabolism. Second, it ensures that modification occurs only to the thioesterified amino acid and not on the free cellular pool. As more biosynthetic pathways are sequenced, it is expected that this mechanism of amino acid modification will be repeated because the NRPS scaffolds are shown to function not only in peptide synthesis but also in amino acid modification during secondary metabolism.

Significance

Pyrrole moieties are found in a number of medically and agriculturally important natural products. Prior precursor labeling studies suggested the pyrrole moieties of coumermycin A_1 and pyoluteorin, as well as one of the pyrroles of undecylprodigiosin, are derived from L-proline. The work presented here characterizes the conversion of the pyrrolidine ring of proline to a pyrrole by enzymes encoded within the undecylprodigiosin and pyoluteorin biosynthetic pathways. It is assumed that homologs from the coumermycin A_1 biosynthetic pathway will work in a similar manner. This conversion involves the activation of L-proline to L-prolyl-AMP by enzymes that are homologous to A domains of NRPSs and the subsequent thioesterification of the amino acids to a protein showing homology with PCP domains of NRPSs. The initial step of proline oxidation is catalyzed by enzymes showing homology to acyl-CoA dehydrogenases and results in the generation of pyrrolyl-2-carboxyl-*S*-PCP. The coordinated action of these three proteins presents a new mechanism for pyrrole moiety biosynthesis. This work is another example of a natural product biosynthetic pathway that uses an NRPS-like scaffold to tether an amino acid for downstream modification.

Experimental Procedures

Cloning of SC3F7.09, SC3F7.11, *redW*, *pltF*, *pltE*, and *pltL* Genes

The genes encoding SC3F7.09 (ORF9), SC3F7.11 (ORF11), and RedW were PCR amplified from *S. coelicolor* A(3)2 strain CH999 (a gift from C. Khosla) genomic DNA. The primers used for the amplification of each gene are listed in Table 4. All three PCR products were cloned into pET37b via the corresponding NdeI and HindIII restriction sites and generated C-terminally His8-tagged proteins when expressed. The resulting plasmids were pORF9-H8, pORF11-H8, and pRedW-H8. Cloning of ORF9 in this manner resulted in an expression vector that did not have a drug resistance marker compatible with pREP4-Sfp. Therefore, the ORF09 gene was subcloned from pORF9-H8 into pET22b via the NdeI and XhoI restriction sites and generated the expression plasmid pORF9-H6, expressing a protein with a C-terminal His6 tag.

The genes encoding PltF, PltE, and PltL were PCR amplified from plasmids (gifts from J. Loper) containing portions of the pyoluteorin biosynthetic cluster. *pltE* and *pltF* were PCR amplified from pJEL5571, whereas *pltL* was PCR amplified from pJEL5912. The primers used for the amplification of each gene are listed in Table 4. The PCR products of *pltF* and *pltE* were digested with NdeI and HindIII and cloned into the corresponding restriction sites of pET37b, resulting in the expression of C-terminally His8-tagged proteins. The resulting vectors were pPltF-H8 and pPltE-H8. The PCR product of *pltL* was digested with NdeI and XhoI and cloned into the corresponding restriction sites of pET22b, resulting in the expression of a C-terminally His8-tagged protein. The resulting plasmid was pPltL-H6.

Heterologous Expression of Proteins in *Escherichia coli*

The expression constructs from both the undecylprodigiosin and pyoluteorin clusters were individually transformed into *E. coli* BL21(DE3) for overexpression and purification. For pORF9-H6 and pPltL-H6, an additional transformation was done to introduce the plasmids into *E. coli* BL21(DE3)/pREP4-Sfp for coexpression with Sfp. Cells harboring the necessary plasmid(s) were grown in LB medium (3 × 1 liter batches) with 100 μg/ml of ampicillin, and kanamycin was added to 50 μg/ml during the coexpression of Sfp with ORF9 and PltL. All cells were grown at 25°C to an OD_{600} of 0.5, cooled to 15°C, and grown 2 hr, then induced with 60 μM (final concentration) isopropyl-D-thiogalactopyranoside (IPTG) and grown an additional 14 hr at 15°C. Cells were harvested by centrifugation (10 min at 10,000 rpm, Sorvall RC5B centrifuge, SLA-3000 rotor), and the 3 × 1 liter batches were pooled and frozen at −20°C until use. For each 3 × 1 liter batch of overexpressing cells, 20 g (wet weight) was recovered.

Purification of ORF9, ORF11, PltF, and PltL

Frozen *E. coli* BL21(DE3) cells containing pORF9-H6 (with or without pREP4-Sfp), pORF11-H8, pPltF-H8, or pPltL-H6 (with or without pREP4-Sfp) were thawed and resuspended in 40 ml of 1× bind buffer (20 mM Tris-HCl [pH 7.9], 500 mM NaCl, and 5 mM imidazole). Resuspended cells were broken by sonication (Fisher 550 Sonic Dismembrator, power = 5, 10 min sonication with 2 s on, 2 s off) and cell debris was removed by centrifugation (30 min at 15,000 rpm, Sorvall RC5B centrifuge, SS-34 rotor). The supernatant was incubated with 2 ml of His•Bind resin (Novagen) for 2 hr at 4°C with gentle rocking. The resin was recovered, washed with 40 ml of 1× bind buffer, packed into a column, and washed with 20 ml of 1× wash buffer (20 mM Tris-Cl [pH 7.9], 500 mM NaCl, and 60 mM imidazole). Protein was eluted with a linear gradient of 100% 1× wash buffer to 100% 1× elution buffer (20 mM Tris-Cl [pH 7.5], 500 mM NaCl, and 500 mM imidazole) over 100 ml. The wash with 1× wash buffer and protein elution were done at a flow rate of 1 ml/min. Fractions containing the target protein (judged by SDS-PAGE) were pooled and dialyzed against buffer A (50 mM Tris-Cl [pH 8.0] at 4°C, 100 mM NaCl, and 10% [v/v] glycerol).

Dialyzed protein was loaded onto a 5 ml Hi-Trap Q Sepharose HP column preequilibrated with buffer A. All ion exchange chromatography steps were performed at a flow rate of 5 ml/min. The column was washed with 50 ml of buffer A, and protein was eluted with a linear gradient of 100% buffer A to 100% buffer B (50 mM Tris-Cl [pH 8.0] at 4°C, 500 mM NaCl, and 10% [v/v] glycerol) over 100 ml. Fractions containing the protein of interest (judged by SDS-PAGE) were pooled and dialyzed overnight against buffer C (50 mM Tris-Cl [pH 8.0] at 4°C, 100 mM NaCl, and 10% [v/v] glycerol). Protein was concentrated with either Centriprep 10 (Amicon) or Centriprep 3 (Amicon) for either ORF11 and PltF or ORF9 and PltL, respectively. Proteins were flash frozen in liquid nitrogen and stored at −80°C. The protein concentration was determined spectrophotometrically at 280 nm by the use of the calculated molar extinction coefficient for each protein: ORF11 (62,430 $M^{-1}cm^{-1}$), ORF9 (8,370 $M^{-1}cm^{-1}$), PltF (54,540 $M^{-1}cm^{-1}$), and PltL (8,370 $M^{-1}cm^{-1}$).

Purification of RedW and PltE

Frozen cells of *E. coli* BL21(DE3) harboring pRedW-H8 were thawed and resuspended in 40 ml of buffer D (50 mM Tris-Cl [pH 8.0] at 4°C, 300 mM NaCl, 10% [v/v] glycerol, 1 mM ethylenediaminetetraacetic acid [EDTA], 200 μM phenylmethylsulfonyl fluoride [PMSF]). Resuspended cells were broken by sonication (Fisher 550 Sonic Dismembrator, power = 5, 10 min sonication with 2 s on, 2 s off), and cell debris was removed by centrifugation (30 min at 15,000 rpm, Sorvall RC5B centrifuge, SS-34 rotor). The supernatant was recovered, and ammonium sulfate precipitation was performed. RedW was found to precipitate between 20%–40% (saturated) based on SDS-PAGE. The 20%–40% pellet was resuspended and dialyzed overnight in buffer D. The dialyzed protein was purified further by Hi-Trap Q Sepharose HP ion exchange chromatography. Prior to being loaded on the column, the protein was diluted with buffer containing 50 mM Tris-Cl (pH 8.0) at 4°C, 10% (v/v) glycerol until the final NaCl concentration of the sample was at 100 mM. The protein was immediately loaded onto the column (5 ml column volume), and the column was washed with 50 ml of buffer A. RedW was eluted with a linear gradient of 100% buffer A to 100% buffer B over 100 ml. Fractions containing RedW (judged by SDS-PAGE) were pooled and dialyzed overnight against buffer A. All ion exchange chromatography steps were done at a flow rate of 5 ml/min. RedW was not soluble when NaCl concentrations fell below 300 mM or glycerol concentration fell below 10% (v/v) glycerol. Thus, overnight dialysis against buffer A resulted in RedW precipitation. Precipitated RedW was recovered by centrifugation (10 min at 10,000 rpm, Sorvall RC5B centrifuge, SS-34 rotor). Protein pellet was resuspended in buffer D, and protein was flash frozen in liquid nitrogen and stored at −80°C. Protein concentration was determined by Bio-Rad Protein Assay with BSA as a standard.

Frozen cells of *E. coli* BL21 (DE3) harboring pPltE-H8 were thawed and resuspended in 40 ml of buffer E (25 mM Tris [pH 8.0], 400 mM NaCl, 2 mM imidazole, and 1 mM FAD). Resuspended cells were broken by sonication (Fisher 550 Sonic Dismembrator, power = 5, 10 min sonication with 2 s on, 2 s off), and cell debris was removed by centrifugation (30 min at 15,000 rpm, Sorvall RC5B centrifuge, SS-34 rotor). The supernatant was incubated with 1 ml of Ni-NTA Superflow nickel resin (Qiagen) for 2 hr at 4°C. The resin was washed with 20 ml of buffer E and then packed into a column. The protein was eluted with a step gradient of increasing imidazole concentration (5, 20, 40, 60, and 200 mM) in buffer E lacking FAD. PltE eluted at 200 mM based on SDS-PAGE. Eluted protein was dialyzed overnight in buffer D lacking EDTA and PMSF, flash frozen in liquid nitrogen, and stored at −80°C. Protein concentration was determined by the calculated molar extinction coefficient (31,760 $M^{-1}cm^{-1}$).

ATP-[^{32}P]PP_i Exchange Assays for Aminoacyl-AMP Formation

Reactions (100 μl) for determining substrate specificity contained 75 mM Tris-Cl (pH 7.5), 10 mM $MgCl_2$, 5 mM Dithiothreitol, 3.5 mM ATP, 5 mM amino acid substrate, and 1 mM [^{32}P]PP_i (0.55 Ci/mol, DuPont NEN) and were carried out at 25°C. The reactions were initiated by the addition of ORF11 or PltF to a final concentration of 50 nM. Reactions were incubated for 10 min and then quenched with charcoal suspensions (500 μl of 1.6% [w/v] activated charcoal, 4.5% [w/v] tetrasodium pyrophosphate, and 3.5% [v/v] perchloric acid). The charcoal pellet was pelleted by centrifugation, washed twice with quenching buffer lacking charcoal, and then resuspended in 0.5 ml of water and submitted for liquid scintillation counting. For the determination of kinetic parameters of L-proline activation, 100 μl reaction mixtures containing 75 mM Tris-Cl (pH 7.5), 10 mM $MgCl_2$, 5 mM dithiothreitol, 3.5 mM ATP, 1 mM [^{32}P]PP_i (2.15 Ci/mol, DuPont NEN), and varying concentrations of L-proline (0.2, 0.5, 1, 3, 5, 10, 15, and 25 mM) were carried out at 25°C. Reactions were started by the addition of either ORF11 (50 nM) or PltF (46 nM) and were terminated after either 10 min (ORF11) or 7 min (PltF). With less than 10% conversion of substrate to product, these conditions were within the linear range of enzyme concentration and enzyme turnover. Data were fit with the Michaelis-Menten equation adjusted for substrate inhibition. For each L-proline concentration, triplicate assays were performed.

TCA Precipitation Assays to Monitor Holo-ORF9 and Holo-PltL Aminoacylation

[^{14}C]-L-proline incorporation into holo-PCPs was monitored with trichloroacetic acid (TCA) precipitation radioassays. A time course for the aminoacylation of the holo-PCPs by each of the L-prolyl-AMP ligases involved a 500 μl reaction mixture containing 75 mM Tris-Cl (pH 7.5), 10 mM $MgCl_2$, 5 mM ATP, 1 mM Tris-(2-carboxyethylphosphine) (TCEP, Sigma), and 0.75 mM [^{14}C] L-proline (8.7 Ci/mol, DuPont NEN) and included 50 nM L-prolyl-AMP ligase (ORF11 or PltF) and 10 μM holo-PCP (ORF09 or PltL). Samples of 50 μl were removed at 5, 10, 15, 20, 25, 30, 45, and 60 min and added to 200 μl of 10% TCA. Protein was pelleted by centrifugation, washed twice with 10% TCA, and resuspended in 88% formic acid, and radiolabeled product was counted by liquid scintillation counting. The percent modification of the PCP domain was calculated from the specific activity of the [^{14}C]L-Proline and the PCP concentration. For determination of the kinetic parameters of holo-ORF9 aminoacylation by the ORF11, 50 μl reactions containing 75 mM Tris-Cl (pH 7.5), 10 mM $MgCl_2$, 5 mM ATP, 1 mM TCEP, 0.75 mM [^{14}C] L-proline (8.6 Ci/mol), 12 nM ORF11, and varying concentrations of holo-ORF09 (1, 2.5, 5, 7.5, 10, 20, 30, and 42 μM) were incubated at 25°C for 10 min. Proteins were precipitated and washed, and scintillation was counted as described above. With less than 10% conversion of substrate to product, these conditions were within the linear range of enzyme concentration and enzyme turnover. Data were fit with the Michaelis-Menten equation with substrate inhibition. For each holo-ORF9 concentration, duplicate assays were performed. For determination of the kinetic parameters of PltL aminoacylation by PltF, 50 μl reactions containing 75 mM Tris-Cl (pH 7.5), 10 mM $MgCl_2$, 5 mM ATP, 1 mM TCEP, 0.75 mM [^{14}C] L-proline (7.2 Ci/mol), 5 nM PltF, and varying concentrations of holo-PltL (2.5, 5, 7.5, 10, 20, 30, 50, and 75 μM) were incubated at 25°C for 5 min. PltF aminoacylation was monitored as described above. With less than 10% conversion of substrate to product, these conditions were within the linear range of enzyme concentration and enzyme turnover, and data were fit with the Michaelis-Menten equation. For each holo-PltL concentration, duplicate assays were performed.

High-Performance Liquid Chromatography (HPLC) Analysis of Purified Apo- and Holo-PCPs

ORF9 and PltL that had been purified after expression in the presence or absence of Sfp were analyzed for 4′-phosphopantetheinylation by HPLC (Beckman System Gold). Apo- and holo-protein were separated with a Vydac Protein and Peptide C18 column at a flow rate of 0.5 ml/min. The following solvents were used: solvent A—15% (v/v) 2-propanol, 0.1% trifluoroacetic acid (TFA) (v/v) in ddH_2O; and solvent B—75% (v/v) 2-propanol, 0.1% TFA (v/v) in ddH_2O. 7.5 nmols of each purified protein were injected for each run. The profile for separation was 5 min isocratic development at 100% A; 20 min linear gradient from 100%A/0%B to 60%A/40%B; and 20 min isocratic development at 60%A/40%B. The elution of the proteins was monitored at A_{280}.

HPLC Analysis of RedW Flavin Cofactor

A 50 μl sample of purified RedW protein (70 μM) was boiled for 5 min, and denatured protein was removed by centrifugation. The flavin present in the supernatant was analyzed by HPLC with a Vydac C18 small-pore column at a flow rate of 1 ml/min. The following solvents were used: solvent C—ddH_20 and 0.1% TFA; and solvent D—acetonitrile and 0.1% TFA. The profile for product separation was 30 min linear gradient from 100%C/0%D to 70%C/30%D. Product elution was monitored at A_{445}.

Assays for the Detection of Pyrrolyl-2-Carbarboxylate Formation by RedW and PltE

The RedW reaction (500 μl) contained 75 mM Tris-Cl (pH 7.5), 10 mM $MgCl_2$, 2 mM TCEP, 300 mM NaCl, 10% (v/v) glycerol, 10 mM L-proline, 15 μM ORF9, 120 nM ORF11, and 8 μM RedW. The reaction was started by the addition of 5 mM ATP and incubated at 25°C for 1 hr. The reaction was terminated by the addition of 1 ml of 10% TCA, and precipitated protein was pelleted by centrifugation. The protein pellet was washed twice with 1 ml of water, resuspended in 200 μl of 0.1 M KOH, and incubated at 65°C. After 15 min, 20 μl

of 50% TFA was added, and precipitated protein was removed by centrifugation. Released products were analyzed by HPLC (discussed below).

The PltE reaction (500 μl) contained 75 mM Tris-Cl (pH 7.5), 10 mM $MgCl_2$, 2 mM TCEP, 10 mM L-proline, 100 μM FAD, 15 μM PltL, 120 nM PltF, and 8 μM PltE. The reaction was started by the addition of 5 mM ATP and incubated at 25°C for 2 hr. The reaction was terminated by the addition of 1 ml of 10% TCA, and precipitated protein was pelleted by centrifugation. The protein pellet was washed twice with 1 ml of water, resuspended in 200 μl of 0.1 M KOH, and incubated at 65°C. After 15 min, 20 μl of 50% TFA was added, and precipitated protein was removed by centrifugation. Released products were detected by HPLC. Separation of the formed products involved HPLC with a Vydac C18 small-pore column at a flow rate of 1 ml/min. The solvents used were as described for RedW flavin analysis. The profile for product separation was 30 min linear gradient from 100%C/0%D to 0%C/100%D. Product elution was monitored at A_{260}.

^{1}H NMR Analysis of RedW Pyrrolyl-2-Carboxylate Product

A large-scale reaction (14 ml) containing 75 mM Tris-Cl (pH 7.5), 10 mM $MgCl_2$, 5 mM ATP, 10 mM L-Proline, 10% (v/v) glycerol, 300 mM NaCl, 10 mM Ferricenium hexafluorophosphate, 10 μM FAD, 2 mM TCEP, 350 μM holo-ORF9, 1 μM ORF11, and 9 μM RedW was incubated at 25°C in 500 μl aliquots for 2 hr. Five hundred milliliters of 10% (w/v) TCA was added to each aliquot to precipitate protein and covalently bound product. The protein pellets were each washed twice with 1 ml of ddH_2O and then resuspended with 1 ml of 0.1 M KOH. The reactions were incubated at 65°C for 15 min and neutralized with TFA, and protein was removed by filtration through Centricon 3 columns. The resulting hydrolyzed products were separated by HPLC according to the protocol described above, and the putative pyrrolyl-2-carboxylate product was collected, lyophilized, resuspended in deuterated methanol, and analyzed by ^{1}H NMR. ^{1}H NMR spectroscopy was performed in a Varian Innova 500 MHz system (TMS d = 0) with a Wilmad microprobe tube.

Synthesis of 1H-pyrrole-2-Carbothioic Acid (Pyrrolyl-2-Carboxyl-*N*-Acetylcysteamine Thioester)

Pyrrolyl-2-carboxylic acid (150 mg, 1.35 mmol) and oxalyl chloride (177 ml, 2.03 mmol) were refluxed in dry dichloromethane (100 ml) for 2 hr. The product was evaporated to dryness, and then N-acetylcysteamine (431 ml, 4.05 mmol) and dry dichloroethane (50 ml) was added. The solution was refluxed overnight and then evaporated to dryness. The product was purified via preparative thin-layer chromatography with a mixture of hexane and ethyl acetate (1:1) to yield 120 mg (42% yield). Results from ^{1}H NMR ($CDCl_3$, 200 MHz) analysis were as follows: δ 1.61 (s, 3H, CH_3CO), 2.74 (m, 2H, CH_2), 3.59 (dd, J = 6.2, 12.9 Hz, 2H, CH_2S), 6.23 (m, 1H, py), 6.57 (m, 1H, py), and 6.92 (m, 1H, py). MALDI-MS analysis of the product found a mass of 213.125 (calculated 213.070) for $C_9H_{12}N_2O_2S$ ($M\text{-}H^+$) .

Mass Analyses of Apo- and Holo-PCPs

For determination of the mass of the apo- and holo-PCP domains, purified protein was prepared for Matrix-assisted laser desorption ionization time-of-flight mass spectral (MALDI-TOF MS) analysis with ZipTip C4 (Millipore) sample preparations. ZipTips were equilibrated with ddH_2O, protein was loaded, washed with ddH_2O, and eluted with 3,5-dimethoxy-4-hydroxycinnamic acid (10 mg/ml). To distinguish between apo- and holo-ORF9, we performed a second MALDI-TOF analysis on HPLC-purified protein.

Acknowledgments

We thank Dr. Joyce E. Loper of Oregon State University and Horticultural Crops Research Laboratory, USDA Agricultural Research Service for the generous gift of plasmids pJEL5571 and pJEL5912 and Dr. Chaitan Khosla of Stanford University for *Streptomyces coelicolor* A3(2) strain CH999. We thank Dr. Colin Thorpe of the University of Delaware for helpful discussions on acyl-CoA dehydrogenases and Dr. Huawei Chen for helpful discussions about this work. This work was supported by National Institutes of Health grant GM 20011 to C.T.W. Both M.G.T. and M.D.B. were supported by National Institutes of Health Postdoctoral Fellowships.

Received: August 7, 2001
Revised: October 2, 2001
Accepted: October 4, 2001

References

1. Maxwell, A. (1993). The interaction between coumarin drugs and DNA gyrase. Mol. Microbiol. *9*, 681–686.
2. Maxwell, A. (1997). DNA gyrase as a drug target. Trends Microbiol. *5*, 102–109.
3. Kirner, S., Hammer, P.E., Hill, D.S., Altmann, A., Fischer, I., Weislo, L.J., Lanahan, M., van Pee, K.H., and Ligon, J.M. (1998). Functions encoded by pyrrolnitrin biosynthetic genes from *Pseudomonas fluorescens*. J. Bacteriol. *180*, 1939–1943.
4. van Pee, K.H., and Ligon, J.M. (2000). Biosynthesis of pyrrolnitrin and other phenylpyrrole derivatives by bacteria. Nat. Prod. Rep. *17*, 157–164.
5. Nowak-Thompson, B., Chaney, N., Wing, J.S., Gould, S.J., and Loper, J.E. (1999). Characterization of the pyoluteorin biosynthetic gene cluster of *Pseudomonas fluorescens* Pf-5. J. Bacteriol. *181*, 2166–2174.
6. Yamamoto, C., Takemoto, H., Kuno, K., Yamamoto, D., Tsubura, A., Kamata, K., Hirata, H., Yamamoto, A., Kano, H., Seki, T., et al. (1999). Cycloprodigiosin hydrochloride, a new H(+)/Cl(−) symporter, induces apoptosis in human and rat hepatocellular cancer cell lines in vitro and inhibits the growth of hepatocellular carcinoma xenografts in nude mice. Hepatology *30*, 894–902.
7. Tsao, S.W., Rudd, B.A., He, X.G., Chang, C.J., and Floss, H.G. (1985). Identification of a red pigment from *Streptomyces coelicolor* A3(2) as a mixture of prodigiosin derivatives. J. Antibiot. *38*, 128–131.
8. Furstner, A., Grabowski, J., Lehmann, C.W., Kataoka, T., and Nagai, K. (2001). Synthesis and biological evaluation of nonylprodigiosin and macrocyclic prodigiosin analogues. ChemBioChem *2*, 60–69.
9. Jordan, P.M. (1994). Highlights in haem biosynthesis. Curr. Opin. Struct. Biol. *4*, 902–911.
10. Gottschalk, G. (1986). Bacterial Metabolism (New York: Springer-Verlag New York Inc.).
11. Scannell, J., and Kong, Y.L. (1969). Biosynthesis of coumermycin A_1: incorporation of L-proline into the pyrrole groups. Antimicrob. Agents Chemother. *9*, 139–143.
12. Wasserman, H.H., Shaw, C.K., and Sykes, R.J. (1974). The biosynthesis of metacycloprodigiosin and undecylprodigiosin. Tetrahedron Lett. *33*, 2787–2790.
13. Wasserman, H.H., Skles, R.J., Peverada, P., Shaw, C.K., Cushley, R.J., and Lipsky, C.R. (1973). Biosynthesis of prodigiosin. Incorporation patterns of C-labeled alanine, proline, glycine, and serine elucidated by fourier transform nuclear magnetic resonance. J. Am. Chem. Soc. *95*, 6874–6875.
14. The Sanger Institute (http://www.sanger.ac.uk/Projects/S_coelicolor/).
15. Wang, Z.X., Li, S.M., and Heide, L. (2000). Identification of the coumermycin A_1 biosynthetic gene cluster of *Streptomyces rishiriensis* DSM 40489. Antimicrob. Agents Chemother. *44*, 3040–3048.
16. Feitelson, J.S., Malpartida, F., and Hopwood, D.A. (1985). Genetic and biochemical characterization of the red gene cluster of *Streptomyces coelicolor* A3(2). J. Gen. Microbiol. *131*, 2431–2441.
17. Malpartida, F., Niemi, J., Navarrete, R., and Hopwood, D.A. (1990). Cloning and expression in a heterologous host of the complete set of genes for biosynthesis of the *Streptomyces coelicolor* antibiotic undecylprodigiosin. Gene *93*, 91–99.
18. Marahiel, M.A. (1997). Modular peptide synthetases involved in nonribosomal peptide synthesis. Chem. Rev. *97*, 2651–2673.
19. Keating, T.A., and Walsh, C.T. (1999). Initiation, elongation, and termination strategies in polyketide and polypeptide antibiotic biosynthesis. Curr. Opin. Chem. Biol. *3*, 598–606.
20. Stachelhaus, T., Mootz, H.D., and Marahiel, M.A. (1999). The

specificity-conferring code of adenylation domains in nonribosomal peptide synthetases. Chem. Biol. *6*, 493–505.
21. Challis, G.L., Ravel, J., and Townsend, C.A. (2000). Predictive, structure-based model of amino acid recognition by nonribosomal peptide synthetase adenylation domains. Chem. Biol. *7*, 211–224.
22. Santi, D.V., Webster, R.W., Jr., and Cleland, W.W. (1974). Kinetics of aminoacyl-tRNA synthetases catalyzed ATP-PPi exchange. Methods Enzymol. *29*, 620–627.
23. Mootz, H.D., and Marahiel, M.A. (1997). The tyrocidine biosynthesis operon of *Bacillus brevis*: complete nucleotide sequence and biochemical characterization of functional internal adenylation domains. J. Bacteriol. *179*, 6843–6850.
24. Weinreb, P.H., Quadri, L.E.N., Walsh, C.T., and Zuber, P. (1998). Stoichiometry and specificity of in vitro phosphopantetheinylation and aminoacylation of the valine-activating module of surfactin synthetase. Biochemistry *37*, 1575–1584.
25. Ehmann, D.E., Shaw-Reid, C.A., Losey, H.C., and Walsh, C.T. (2000). The EntF and EntE adenylation domains of *Escherichia coli* enterobactin synthetase: sequestration and selectivity in acyl-AMP transfers to thiolation domain cosubstrates. Proc. Natl. Acad. Sci. USA *97*, 2509–2514.
26. Keating, T.A., Suo, Z., Ehmann, D.E., and Walsh, C.T. (2000). Selectivity of the yersiniabactin synthetase adenylation domain in the two-step process of amino acid activation and transfer to a holo-carrier protein domain. Biochemistry *39*, 2297–2306.
27. Khosla. (1997). Harnessing the biosynthetic potential of modular polyketide synthases. Chem. Rev. *97*, 2577–2590.
28. Stachelhaus, T., Huser, A., and Marahiel, M.A. (1996). Biochemical characterization of peptidyl carrier protein (PCP), the thiolation domain of multifunctional peptide synthetases. Chem. Biol. *3*, 913–921.
29. Quadri, L.E., Weinreb, P.H., Lei, M., Nakano, M.M., Zuber, P., and Walsh, C.T. (1998). Characterization of Sfp, a *Bacillus subtilis* phosphopantetheinyl transferase for peptidyl carrier protein domains in peptide synthetases. Biochemistry *37*, 1585–1595.
30. Lambalot, R.H., Gehring, A.M., Flugel, R.S., Zuber, P., LaCelle, M., Marahiel, M.A., Reid, R., Khosla, C., and Walsh, C.T. (1996). A new enzyme superfamily—the phosphopantetheinyl transferases. Chem. Biol. *3*, 923–936.
31. Gocht, M., and Marahiel, M.A. (1994). Analysis of core sequences in the D-Phe activating domain of the multifunctional peptide synthetase TycA by site-directed mutagenesis. J. Bacteriol. *176*, 2654–2662.
32. Stachelhaus, T., and Marahiel, M.A. (1995). Modular structure of peptide synthetases revealed by dissection of the multifunctional enzyme GrsA. J. Biol. Chem. *270*, 6163–6169.
33. Shaw-Reid, C.A., Kelleher, N.L., Losey, H.C., Gehring, A.M., Berg, C., and Walsh, C.T. (1999). Assembly line enzymology by multimodular nonribosomal peptide synthetases: the thioesterase domain of *E. coli* EntF catalyzes both elongation and cyclolactonization. Chem. Biol. *6*, 385–400.
34. Keating, T.A., Marshall, C.G., and Walsh, C.T. (2000). Reconstitution and characterization of the *Vibrio cholerae* vibriobactin synthetase from VibB, VibE, VibF, and VibH. Biochemistry *39*, 15522–15530.
35. Gehring, A.M., Bradley, K.A., and Walsh, C.T. (1997). Enterobactin biosynthesis in *Escherichia coli*: isochorismate lyase (EntB) is a bifunctional enzyme that is phosphopantetheinylated by EntD and then acylated by EntE using ATP and 2,3-dihydroxybenzoate. Biochemistry *36*, 8495–8503.
36. Redenbach, M., Kieser, H.M., Denapaite, D., Eichner, A., Cullum, J., Kinashi, H., and Hopwood, D.A. (1996). A set of ordered cosmids and a detailed genetic and physical map for the 8 Mb *Streptomyces coelicolor* A3(2) chromosome. Mol. Microbiol. *21*, 77–96.
37. Thorpe, C., and Kim, J.J. (1995). Structure and mechanism of action of the acyl-CoA dehydrogenases. FASEB J. *9*, 718–725.
38. Budzikiewicz, H., Djerassi, C., Jackson, A.H., Kenner, G.W., Newman, D.J., and Wilson, J.M. (1960). Pyrroles and related compounds. Part IV. Mass spectrometry in structural and stereochemical problems. Part XXX. Mass spectra of monocyclic derivatives of pyrrole. J. Chem. Soc., 1949–1960.
39. Hofle, G., and Wolf, H. (1983). Isolierung, 13C-NMR-spektren und biogenese von resistomycin und esistoflavin aus *Streptomyces griseoflavus* B 71 (Actinomycetales). Liebigs Ann. Chem., 835–843.
40. Lehman, T.C., and Thorpe, C. (1990). Alternate electron acceptors for medium-chain acyl-CoA dehydrogenase: use of ferricenium salts. Biochemistry *29*, 10594–10602.
41. Tiffany, K.A., Roberts, D.L., Wang, M., Paschke, R., Mohsen, A.W., Vockley, J., and Kim, J.J. (1997). Structure of human isovaleryl-CoA dehydrogenase at 2.6 Å resolution: structural basis for substrate specificity. Biochemistry *36*, 8455–8464.
42. Stankovich, M.T., Sabaj, K.M., and Tonge, P.J. (1999). Structure/function of medium chain acyl-CoA dehydrogenase: the importance of substrate polarization. Arch. Biochem. Biophys. *370*, 16–21.
43. Kim, J.J., and Wu, J. (1988). Structure of the medium-chain acyl-CoA dehydrogenase from pig liver mitochondria at 3-Å resolution. Proc. Natl. Acad. Sci. USA *85*, 6677–6681.
44. Kim, J.J., Wang, M., and Paschke, R. (1993). Crystal structures of medium-chain acyl-CoA dehydrogenase from pig liver mitochondria with and without substrate. Proc. Natl. Acad. Sci. USA *90*, 7523–7527.
45. Chen, H., and Walsh, C.T. (2001). Coumarin formation in novobiocin biosynthesis: β-hydroxylation of the aminoacyl enzyme tyrosyl-*S*-NovH by a cytochrome P540 NovI. Chem. Biol. *74*, 1–12.
46. Chen, H., Hubbard, B.K., O'Connor, S.E., and Walsh, C.T. (2002). Formation of β-hydroxy histidine in the biosynthesis of nikkomycin antibiotics. Chem. Biol., *9*, 103–112.